sciendo

Polish Journal of Chemical Technology, 25, 4, 10—18, 10.2478/pjct-2023-0033

Experimental research on the removal characteristics of simulated radioactive aerosols by a cloud-type radioactive aerosol elimination system

Jiqing Zhang[1], Ying Jia[1*], Xiaomeng Lv[1], Tiedan Xiong[2], Yuanzheng Huang[1], Keke Shen[1]

[1]College of Missile Engineering, Rocket Force University of Engineering, Xi'an Shannxi 710025, People's Republic of China

[2]School of Marine Science and Technology, Harbin Institute of Technology, Weihai Shandong 264209, People's Republic of China

[*]*Corresponding author: e-mail:* jyingsx@163.com

Radioactive aerosols in the confined workplace are a major source of internal exposure hazards for workers. Cloud-type radioactive aerosol elimination system (CRAES) have great potential for radioactive aerosol capture due to their high adsorption capacity, lack of cartridges and less secondary contamination. A CRAES was designed and constructed, and a FeOOH/rGO composite was directly prepared by a hydrothermal method to characterise and analyse its morphology, chemical structure and removal efficiency for simulated radioactive aerosols. The results show that the FeOOH/rGO composite works in synergy with the CRAES to effectively improve the removal efficiency of simulated radioactive aerosols. A 30-minute simulated radioactive aerosol removal rate of 94.52% was achieved when using the experimentally optimized composite inhibitor amount of 2 mg/L FeOOH/rGO with 0.2 g/L PVA as a surfactant. Therefore, the CRAES coupled with the composite inhibitor FeOOH/rGO has broad application potential for the synergistic treatment of radioactive aerosols.

Keywords: Radioactive aerosols, elimination, composite, CRAES, FeOOH/rGO.

INTRODUCTION

Today's dwindling reserves of fossil resources have led to more attention being paid to nuclear energy as a clean energy source, and research on nuclear energy will be a research hotspot for quite some time to come, while in the military, strategic-grade nuclear weapons are also an important bargaining chip in the game of great powers[1, 2]. Nuclear energy uniquely generates radioactive aerosols in confined workplace during the production and processing of nuclear materials, the operation of nuclear facilities, the storage of nuclear weapons and the decommissioning of nuclear facilities[3, 4]. A radioactive aerosol is a colloidal dispersion of solid or liquid particles suspended in a gaseous medium containing or contaminated with radionuclides, the particle size of which is mainly distributed between 0.01 and 100 microns[5]. The danger of radioactive aerosols cannot be ignored because of their properties as both aerosols and radioactive substances. The ventilation effect in the confined space is poor, and once the radioactive aerosol is formed, it can exist for a long time and easily enter the human body through breathing, so it is the main source of radiation hazards in confined space workers. The harm of radioactive aerosol to the human body is related to particle size[6]. If the particle size exceeds 10 microns, it is deposited in the oral and nasal cavity. If the particle size is between 2.5 microns and 10 microns, it is deposited in the throat and upper bronchi, it eventually dissolves into sputum and is expelled from the body, thus posing less risk of internal exposure. If they are smaller than 2.5 microns in size, aerosols will enter the bronchi and alveoli, causing severe radiation hazard and irreversible damage to organs[1]. Therefore, the effective treatment of radioactive aerosols with a particle size of less than 2.5 microns in working environments is important for the health of workers. Radioactive aerosols are formed by radionuclides adsorbed on the surface of aerosol particles in the air[7], so research in the field of radioactive aerosol removal is currently based on the theory of general aerosol removal.

Current technologies for the removal of radioactive aerosols include physical filtration, electrostatic capture, bubbling washing, atomization capture, pressurised dissolved gas air flotation and spraying inhibitors[8, 9]. The traditional physical filtration fiber has the advantages of mature technology and low cost, and is widely used in the field of air purification. The purification of radioactive aerosol is often accompanied by greater air resistance and the generation of a large number of radioactive filter materials. Dry electrostatic capture technology has the characteristics of high energy consumption and low efficiency, so it needs to be further studied and optimized. Due to its small amount of radioactive solid waste and long service life, wet process technology has attracted the attention of researchers in recent years[10]. Pressurised dissolved gas air flotation equipment is relatively complex and the technology is not mature enough. atomization capture and spraying inhibitors have long operation time, and at present, organic materials are used as the research object, which has limitations. The above technology is accompanied by the generation of a large amount of radioactive waste, which has the biggish potential risk of secondary contamination. In response to the characteristics of radioactive aerosol removal in confined workplaces, the combination of atomization capture technology and aerosol elimination technology has been proposed for the synergistic removal of radioactive aerosols. In this approach, a graphene-based radioactive aerosol inhibitor is prepared and aerosolised, the radioactive aerosols in the air are adsorbed, and the adsorbed condensed particles are passed through a specially designed cloud-type radioactive aerosol elimination system (CRAES) to achieve efficient removal of the radioactive aerosols. Compared to conventional technology, it has a larger adsorption capacity, and the filterless design avoids abundant secondary contamination and enables direct and contained treatment.

FeOOH has been widely used for the adsorption of radioactive wastewater and heavy metal ion wastewater. Wang prepared L-arginine-modified FeOOH (2Arg@FeOOH) for the first time and loaded it on a fibrous membrane (FM) to form 2Arg@FeOOH/FM for the removal of As (V) from contaminated water[11]. Wu synthesised mesoporous FeOOH polycrystalline phenotypes, and the study revealed the reaction mechanism of FeOOH with Cr (VI) and the different behaviour of the four FeOOH polymorphs in the removal of Cr (VI)[12]. Graphene and graphene oxide (GO) are widely used due to their unique structural and morphological characteristics, exhibiting excellent electrical, mechanical and thermal properties[13, 14, 15]. In this study, graphene was used as a substrate to provide more active sites due to its large specific surface area, FeOOH was used as the main active substance, and surfactants were used to reduce the surface tension of droplets and improve the coagulation efficiency[16, 17].

Cloud-air-purifying (CAP), proposed by Wang[18], is based on cloud physics and uses agglomeration growth technology to achieve efficient removal of fine particulate matter. The technology simulates the natural rainfall process by constructing an environment of supersaturated relative humidity through an ultrasound atomization unit, and the induced draught fan unit creates a disturbed flow field in the system. The fine particulate matter in the ultrasound atomization unit is in full contact with the saturated water vapour and acts as condensation nuclei, agglomerating and increasing in particle size; it is then collected efficiently by a modified cyclone separator.

In this study, a CRAES was designed and constructed, a FeOOH/reduced graphene oxide (rGO) composite was prepared and characterised, and the removal effect of different concentrations of composite inhibitor on simulated radioactive aerosols were investigated based on the synergy between the composite inhibitor and the CRAES. To increase the surface activity and improve the coagulation efficiency, the effects of different surfactant types and concentrations on the removal effect were investigated, the optimum ratio of the composite inhibitor for the method was obtained, the removal effect was evaluated, and finally, the removal mechanism was investigated and analysed.

EXPERIMENTAL

Materials

Concentrated sulfuric acid (H_2SO_4, 98 wt.%) and hydrochloric acid (HCl, 37 wt.%) were purchased from Chengdu Kelong Chemical Co., Ltd. Sodium nitrate ($NaNO_3$, V), hydrogen peroxide (H_2O_2, 30 wt.%) and sodium sulfate ($NaSO_4$, VII) were purchased from Sinopharm Chemical Reagent Co., Ltd. Graphite powder, cesium chloride (CsCl, I), polyoxyethylene sorbitan fatty acid ester (Tween-60), hexadecyl trimethyl ammonium bromide (CTAB), polyvinyl alcohol (PVA), sodium dodecyl benzene sulfonate (SDBS) and iron (III) chloride hexahydrate ($FeCl_3 \cdot 6H_2O$) (AR, 99.0%) were purchased from Shanghai Titan Scientific Co., Ltd. Potassium permanganate ($KMnO_4$) was purchased from Harbin City Xinchun Chemical Plant. Deionised (DI) water was laboratory-made. All chemicals were of analytical grade and were used without further purification.

Preparation

GO was prepared by the modified Hummers method[19, 20, 21]. First, 70 mL of concentrated H_2SO_4 was kept below 4 °C in an ice-water bath, and 3 g of graphite powder and 1.5 g of $NaNO_3$ were added under stirring. Then, 9 g of $KMnO_4$ was added in small amounts several times over a period of 1 h to maintain the temperature. The beaker was then shifted to a constant temperature water bath at 35 °C with magnetic stirring for 2 h. A total of 150 mL of DI water was added, The beaker was placed in a constant temperature water bath at 95 °C, and magnetic stirring was performed for 15 min. Afterwards, 500 mL of DI water was added to finish the reaction, and 20 mL of H_2O_2 solution (30 wt.%) was slowly added. The solution was filtered and washed several times by centrifugation with 200 mL of HCl (10 wt.%) and DI water to bring the pH close to neutral. A dispersed suspension of GO was obtained.

The preparation of FeOOH and FeOOH/rGO was achieved by a hydrothermal process[22]. A certain amount of GO was dispersed in 30 mL of DI water by ultrasonic stirring; 0.5406 g $FeCl_3 \cdot 6H_2O$ was added, and the mixture was stirred for 30 min, after which 0.2841 g $NaSO_4$ was added, and the mixture was stirred until completely dispersed. The obtained liquid was kept in a 50 mL autoclave at 120 °C for 6 h. The product was collected by centrifugation and washed several times with DI water to obtain dispersion. FeOOH was synthesised under the same conditions without the addition of GO for comparison.

Characterisation

The samples were characterized using Fourier transform infrared spectroscopy (FT-IR), Raman analysis, and scanning electron microscopy (SEM). The surface functional groups of samples in the range of 400–4000 cm^{-1} were analyzed using FT-IR (Nicolet Is5, Thermo Fisher, USA). A laser confocal Raman spectrometer (Lab RAM HR Evolution, Horiba Scientific) with an excitation wavelength of 633 nm was used to obtain the spectrogram of the sample in the range of 50–2000 cm^{-1}. The surface morphologies were characterised by SEM (Gemini SEM 300, ZEISS, Germany).

Particulate Matter Removal Test

The removal of radioactive aerosols is based on general aerosol decontamination[7], so this experimental method was designed accordingly. The removal experiments were carried out in an environmental simulation chamber with ventilation facilities and dimensions of 2500*2000*2000 mm. Before the start of the experiments, the composite inhibitor solution was added to the atomization system and stirred well. At this time, close the ventilation facilities to ensure that the experimental chamber is airtight. Radioactive aerosols particles were simulated by burning incense. Experiments were started after the aerosols particles concentration distribution had stabilised, in which a homemade CRAES was used for the removal of simulated radioactive aerosols from the environmental simulation chamber. After the end of the experiment,

the CRAES was turned off, the ventilation device was turned on, and the data were derived to complete this round of experiment. The next round of experiment could be started when the concentration of aerosol particles dropped to similar to that in the room.

The particle size was analysed using a spray laser particle size analyser (JL-3000), the PM2.5 mass concentration was monitored by a dust meter (TSI-8533EP, TSI-8530EP, US), and the PM2.5 quantity concentration was monitored using a laser dust particle counter (LX--600S). The removal effect of simulated radioactive aerosols over a certain period of time was evaluated by means of an efficiency equation. The calculation formula is as follows:

$$\eta = \frac{C_0 - C}{C_0} \tag{1}$$

where:

C_0 – mass concentration before purification, μg/m^3;

C – mass concentration after purification, μg/m;

η – purification efficiency, %.

To sum up, the mass concentration measured by the TSI is mainly used as the basis for the calculation of efficiency. Combined with the functional characteristics of the TSI and experimental requirements, the test details are sampled once per second, each test lasts for 1 min, each test interval is 10 min and test particle size is 2.5 microns. The data recorded for 4 times correspond to the initial uniform aerosol distribution, 10 min, 20 min and 30 min after purification, respectively. Finally, the average value of the test is taken to plot.

After completing routine tests to simulate radioactive aerosols, CsCl was used to simulate radioactive aerosol to verify the purification effect of the system. Firstly, a certain amount of CsCl powder was dissolved in water, and the experimental smoke column was soaked in CsCl solution for 24 h and dried at 60 °C. And then we did the experiment in the same way.

CLOUD-TYPE RADIOACTIVITY AEROSOL ELIMINATION SYSTEM

Ultrasound atomization unit

The atomization unit is a key part of the CRAES (Fig. 1). The constructed environment of supersaturated relative humidity is necessary for the capture of radioactive aerosol particles by the inhibitors. Studies have shown that fine particles are more easily captured when the atomised droplets are of similar particle size to the fine particles and that the best capture is achieved when the ratio of droplet to fine particle size is between 1.25 and 5. Kirpalani investigated the particle size distribution of water in the particle size range of 4 to 10 microns for ultrasonic atomization at a power of 2.47 MHz and temperatures of 283 K and 297 K[23]. The particle size of the droplets obtained by ultrasonic atomization is much smaller than that produced by hydrodynamic methods. Therefore, the CRAES applies ultrasonic atomization to obtain droplets with a particle size similar to that of fine particles, which are more easily agglomerated and enlarged. The droplet particle size distribution is concentrated, which can form a stable atomization field and can control the amount of inhibitor atomization occurring according to different practical situations. The inhibitors solution configured according to the study is placed in the ultrasound atomization unit to achieve contact purification with aerosol particles through atomization.

Cloud-type elimination unit

The cloud-type elimination unit is the core component of the CRAES and is the main location where radioactive aerosol particles are collected. The first capture takes place in the Higee field constituted by the outer cylinder, where the radioactive aerosol particles coupled by adsorption settle rapidly. The inhibitor droplets and dirty air pass through the outer barrel and enter the intermediate barrel along the inlet and outflow holes, where they rotate up the wall and are captured a second time in the second Higee field. The intermediate cylinder consists of a number of small cyclones connected in parallel to form a third supergravity field. The outlet of the cyclone is connected by an elbow, and the purified air is collected at the outlet, where the agglomerated particles are collected along the wall after compaction coupling. In contrast to conventional cyclones, the three-stage Higee field environment provides a graded treatment of radioactive aerosol particles in different particle size ranges that are coupled with inhibitors, changing the movement characteristics of the particles, increasing the contact time and contact area and significantly improving the removal efficiency of radioactive aerosols.

There is a special collection container under the Cloud--type elimination unit to collect the radioactive aerosol particles that are adsorbed by the material, and the radioactive liquid waste is formed here, and then only need to replace the container and pack the container full of the liquid waste. Compared the conventional purification techniques for generating radioactive solid waste, the secondary contamination is smaller, and the radioactive waste disposal technology is more mature. Safety and less secondary contamination are the advantages of this method.

Dehumidification unit

To ensure the desired relative humidity in the purification area, the dehumidification unit was designed by combining the characteristics of the system with actual application conditions. The addition of the dehumidification unit to the purification system resulted in a significant reduction in the relative humidity in the experimental area and solved the practical problem of the solution being drawn into the induced draught fan unit under high wind speed conditions.

Draught fan unit

The draught fan unit is the power source for the entire system, and its main component is the vortex fan, which is used to create a disturbed flow field[24].

Channel

The connection between the system components and the formation of the entire flow field rely on piping. Based on the design objectives of corrosion resistance, low cost and ease of maintenance and assembly, a 50 mm

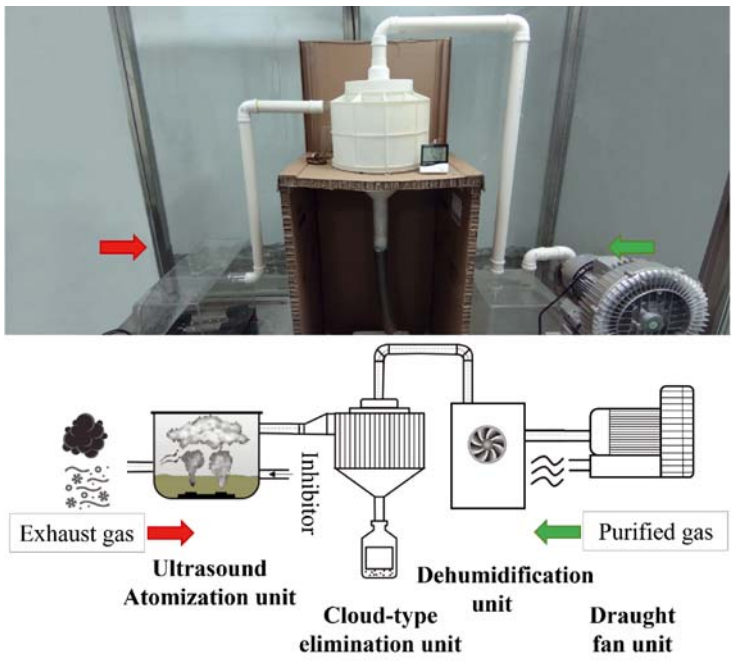


Figure 1. Physical and schematic comparison of the CRAES

PVC pipe was chosen as the piping material to facilitate experiments and practical applications.

The operating parameters of the equipment are shown in Table 1.

Table 1. Operating parameters of the equipment

No.	Parameter	Numerical value
1	Fan power (W)	1100
2	Fan airflow (m^3/h)	180
3	Negative fan pressure (kPa)	24
4	Blower air pressure (kPa)	30
5	Fogging volume (kg/h) (H_2O)	12

RESULTS AND DISCUSSION

Characterisation

The SEM image of FeOOH shown in Fig. 2(a) is an approximately spherical flower-like shape composed of nanorods, which grow uniformly from the center of the particle. GO, as shown in Fig. 2(b), exhibited a laminated stacked structure with slight agglomeration. It grows uniformly from the center of the particle. In addition, the FeOOH-rGO SEM image, shown in Fig. 2(c), shows the distribution of rGO thin layers on FeOOH particles, which indicates the successful binding of rGO and FeOOH, which confirms the results of previous studies[20].

To further understand the distribution of FeOOH and rGO, the EDS energy spectrum sweeping diagram as shown in Fig.3 shows that C and Fe are evenly distributed under a scale of 1μm, and rGO is wrapped on FeOOH, where the mass fraction of C is 20.78%, the mass fraction of Fe is 46.39%, and the mass fraction of O is 32.83%. Further proof of the successful combination of FeOOH and rGO.

The Raman spectra of the prepared GO and FeOOH/rGO composite with mainly D and G peaks are shown in Fig. 4. GO exhibited Raman shifts corresponding to the D and G bands at 1349.67 cm^{-1} and 1593.75 cm^{-1}, respectively, as well as an intensity ratio between the D and G bands (ID/IG) of 0.851. In the Raman spectra of the FeOOH/rGO composite, in addition to the unique peaks assigned to FeOOH, the D-band and G-band of rGO appear at 1352.85 cm^{-1} and 1592.21 cm^{-1}, respectively, with an ID/IG value of 0.981. The increased ID/IG value of FeOOH-rGO compared to GO confirms the reduction of GO to rGO in the composite[25, 26]. The vibrational intensity of the D and G peaks of rGO is increased compared to that of GO, while there is more disorder between the rGO lamellae. The chemical bonds formed between the rGO lamellae and FeOOH lead to a shift and change in the relative intensity of the peaks at 1349.67 cm^{-1} and 1593.75 cm^{-1}.

To further analyse the surface groups of the FeOOH/rGO composite, FT-IR was used (Fig. 5). The peaks of 1731 cm^{-1} and 1617 cm^{-1} on GO correspond to the C = O bond extension of the carbonyl or carboxyl group on GO and the deformation of the hydrogen/oxygen

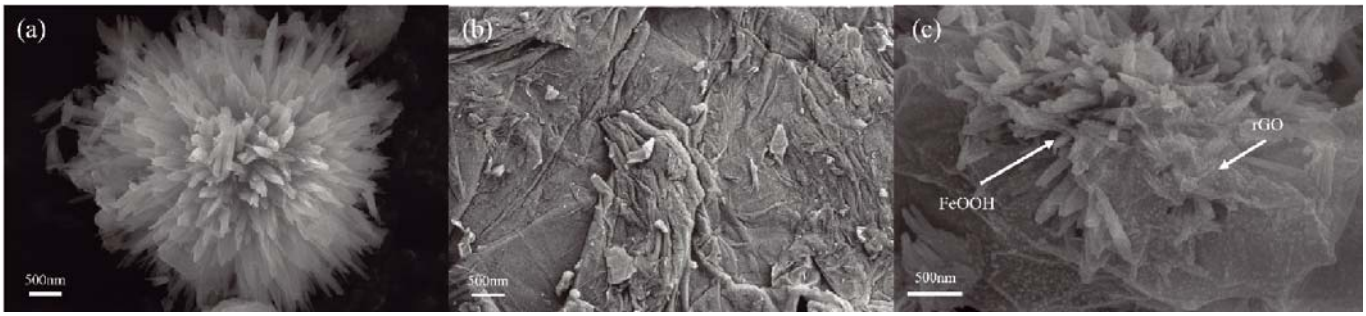


Figure 2. SEM images of FeOOH (a), GO (b) and FeOOH/rGO (c)

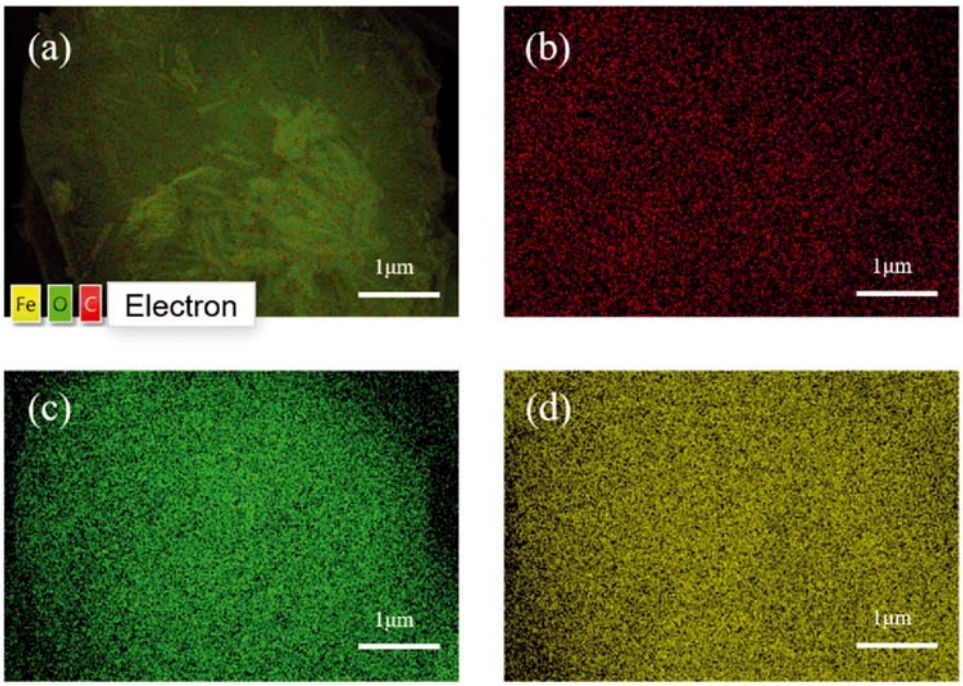


Figure 3. EDS spectrum of FeOOH/rGO. (a) stratified image, (b) C Kα1,2, (c) O Kα1, (d) Fe Kα1

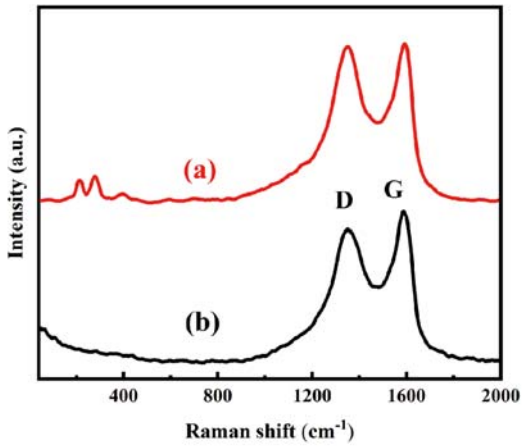


Figure 4. Raman spectra of FeOOH/rGO (a) and GO (b)

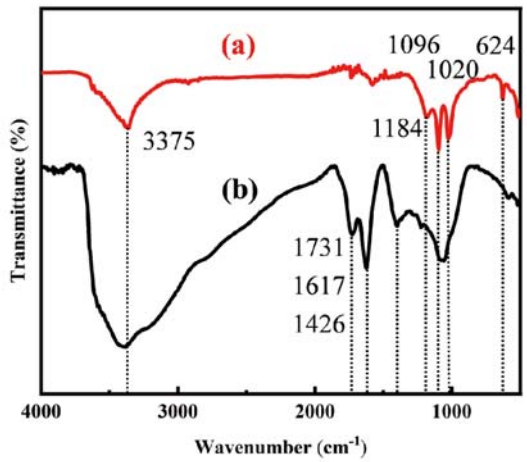


Figure 5. FT-IR spectra of FeOOH/rGO (a) and GO (b)

bond in water, respectively[27]. The peak near 1068 cm^{-1} corresponds to the contraction vibration of C – O – C in the cyclooxygen group[28], and the absorption peak of the symmetric contraction vibration of carboxyl group (– COO –) is near 1426 cm^{-1} [29]. Peaks near 1617 cm^{-1} correspond to the presence of epoxy groups and the stretching vibration of C = C, indicating the presence of carboxyl and epoxy groups in GO[30]. The 3375 cm^{-1} and 624 cm^{-1} absorption bands are characteristic of -OH, where 3375 cm^{-1} is the vibrational absorption band of -COOH and the peak intensity of the carboxyl group is diminished, showing that the surface of GO was reduced to produce rGO. The peaks at 1096 cm^{-1} and 1020 cm^{-1} can be attributed to the vibration of Fe-O in FeOOH, confirming the successful preparation of FeOOH[31].

Establishment of experimental methods

Burning incense in the experimental chamber was used to simulate radioactive aerosols, and the system was set to TSI acquisition mode. The variation curve of particulate matter mass concentration in the experimental chamber was obtained (Fig. 6). The incense was lit at 0 min and burned out at 10 min, and the mass concentration reached a maximum at 12 min and dropped steeply at 14 min, as shown in the graph. Multiple parallel experiments were analysed and it was concluded that due to the smoke density and the monitoring position setting, after burning out, a large amount of particulate matter was

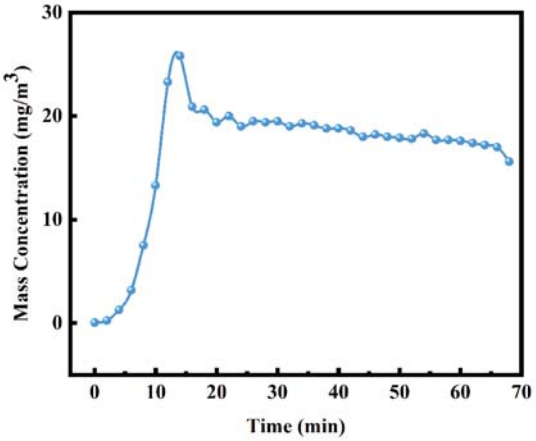


Figure 6. Change in particulate matter mass concentration

deposited at the test position, resulting in a high local mass concentration. After 2 min, the particulate matter was evenly distributed throughout the experimental chamber, and the mass concentration stabilised, showing a slight downward trend. To ensure the accuracy of the data, the removal effect experiment was started 10 min after burning out.

Particulate matter removal test

In the experiment monitoring natural aerosol sedimentation from 0–60 min (Fig. 7), the 60 min natural sedimentation rate was only 7.7%. When the system was used, the 30 min removal rate reached 93.04%. In 30 minutes, the high concentration (> 10000 μg/m^3) of PM 2.5 was reduced to less than 1000 μg/m^3 and continued to decrease. However, the removal efficiency increased after 40 min. After the analysis of several monitoring sessions, it was concluded that the system could operate for up to 40 min. Due to the continuous work of the atomization system, the content of fine particulate matter in the air dropped rapidly, causing the oversaturation of water vapour and resulting in water vapour discharge with the circulation system; however, the detection equipment did not have the ability to differentiate the substances, causing the removal rate to rise, which was a system error. However, in actual engineering applications, the mass concentration of particulate matter is much greater than 10 mg/m^{3,} and the volume of confined spaces is much greater than the volume of the experimental chamber. The upper operating limit is much more than 40 min, so there is no substantial impact on engineering applications. To avoid experimental errors, the following experiments tested the removal efficiency within 30 min, calculated the removal rate and evaluated the results.

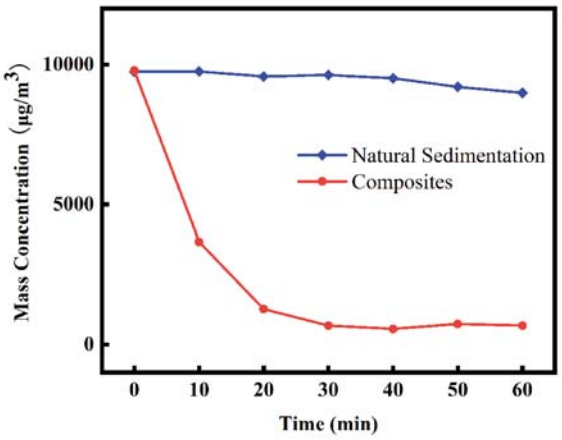


Figure 7. Comparison of natural settling and effect experiments

The CRAES was monitored for 60 min of operation in the experimental chamber for different particle sizes, and the results showed excellent removal of aerosol particles of different particle sizes (Fig. 8). Under laboratory conditions, the CRAES has excellent particle removal capability for PM 1, PM 2.5 and PM 10 with removal efficiencies of 91.62%, 93.04% and 95.24%, respectively.

Water is the base material of the inhibitor, which itself has a certain agglomeration effect on aerosol particles and adsorption effect. To explore the capture effect of the homemade FeOOH/rGO composite, water alone as an inhibitor was compared with water combined with the composite inhibitor (Fig. 9). The results show that

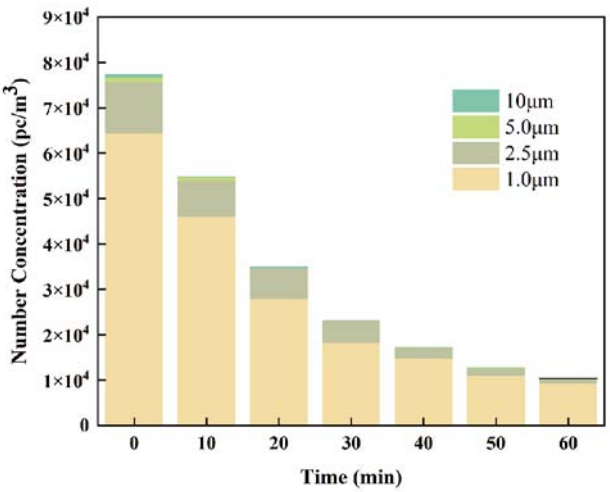


Figure 8. Variation in the number concentration of particles of different particle sizes

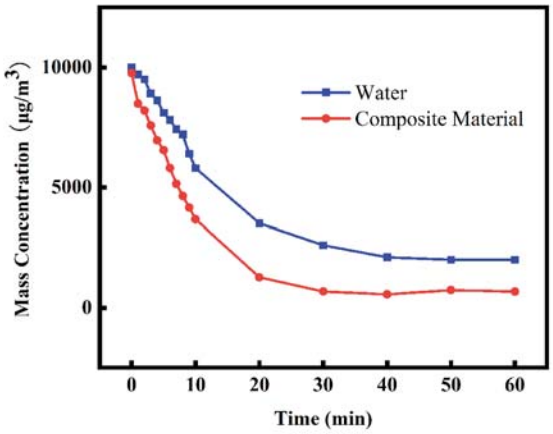


Figure 9. Experimental comparison of water and composite

the homemade CRAES with water as the inhibitor had a good removal effect on PM2.5 with a removal efficiency of 74.21% at 30 min. After adding 2 mg/L FeOOH/rGO composite, the removal efficiency was even higher with a removal rate of 93.04% at 30 min (Fig. 10).

It has been concluded that the homemade FeOOH/rGO composite is effective in removing simulated radioactive aerosols, and experiments were designed to explore the best removal efficiency with different concentrations of composite (Fig. 11). Five groups were prepared with different concentrations of 1 mg/L, 2 mg/L, 5 mg/L, 10 mg/L, and 20 mg/L. The results showed that the removal rates at 30 min were 90.51%, 93.04%, 91.64%, 89.51% and 87.66%, respectively. The highest removal rate of

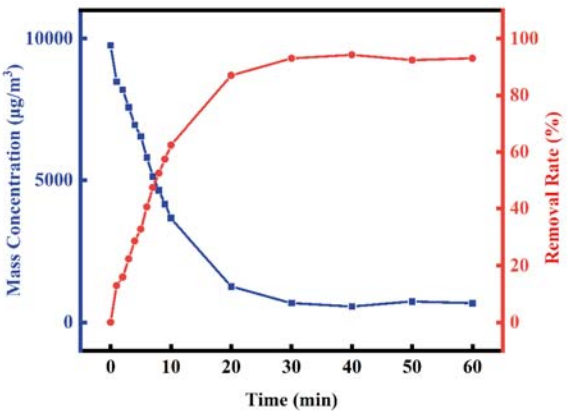


Figure 10. Mass concentration and removal rate over time

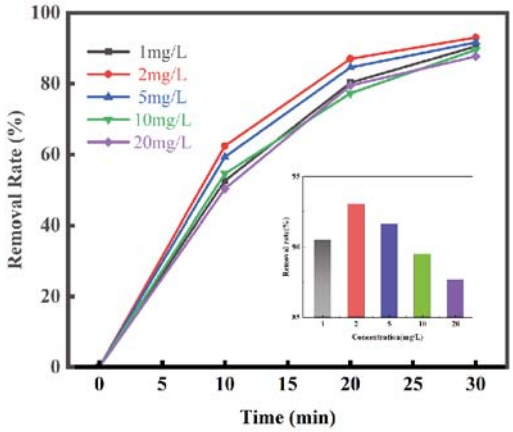


Figure 11. Removal efficiency with different concentrations of composite

93.04% was achieved at 2 mg/L. The removal rate decreased significantly when the concentration was higher than 2 mg/L. A concentration of 1 mg/L was too low, and the removal effect was not satisfactory. Therefore, for these experimental conditions, the optimum FeOOH/rGO composite concentration for the CRAES is 2 mg/L.

According to Fletcher's classical heteronucleation theory, the improvement of particle wettability can reduce the critical susaturation required for heteronucleation and surface tension , thus improving the effect of water vapor phase transition on promoting the growth of fine particles[35, 36]. To increase surface activity and improve coagulation efficiency, the enhancement effect of different surfactants on the removal ability of the FeOOH/rGO composite was tested. Four typical surfactants, an anionic surfactant sodium dodecyl benzene sulfonate (SDBS), the cationic surfactant cetyl trimethyl ammonium bromide (CTAB), the nonionic surfactant Tween-60 (Tween) and the water-soluble polymer surfactant polyvinyl alcohol (PVA) were selected; 0.2 g/L of each of the four surfactants was added to the composite at an optimum concentration of 2 mg/L FeOOH/rGO to compare the enhancement effect (Fig. 12). By calculating the amount of the corresponding surfactant and FeOOH/rGO, stirring evenly to ensure full mixing, the FeOOH/rGO composite inhibitor is obtained in the ultrasound atomization unit. The removal of the simulated radioactive aerosols was tested for 10 min and compared with that achieved with the composite alone. The results showed that the removal rate of the composite alone after 10 min was 62.38%. At this time, Tween was already less efficient than the composite due to its high viscosity at 53.97%, and CTAB, SDBS and PVA were all more efficient to varying degrees, with the 0.2 g/L PVA solution being the most effective at 73.70%.

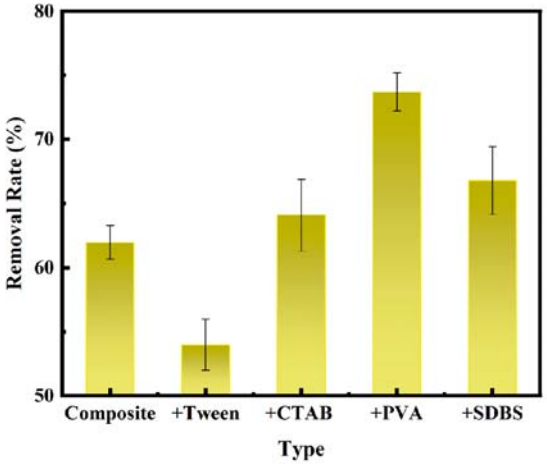


Figure 12. Enhancement effect of different surfactants on the composite effect

By comparing the enhancement effect of four different surfactants, it was determined that PVA had a good enhancement effect. To determine the best concentration to maximize the enhancement effect, experiments were performed to verify the enhancement effect of five different concentrations of PVA solution: 0.1 g/L, 0.2 g/L, 0.3 g/L, 0.4 g/L and 0.5 g/L (Fig. 13). The results showed that 0.2 g/L PVA solution had the best enhancement effect, and the removal efficiency decreased with increasing concentration. Experimental observations indicated that when the concentration is too high, dense foam forms in the ultrasound atomization unit, which affects the atomization effect and causes a decrease in the removal rate, and when the concentration is too low, the particulate matter cannot be fully coagulated.

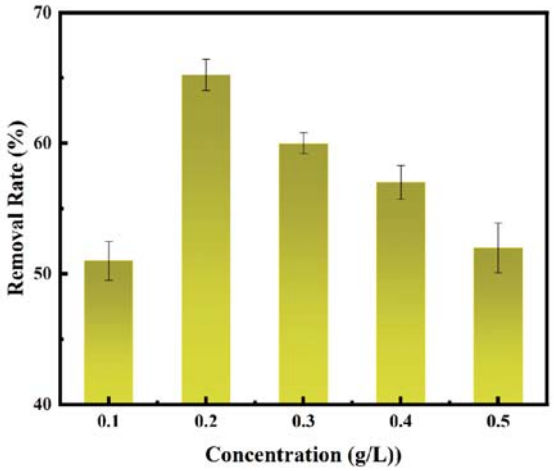


Figure 13. Enhancement effect of different concentrations of PVA surfactant

Finally, the concentration of FeOOH/rGO composite with the best removal effect (2 mg/L) and 0.2 g/L PVA solution were selected to measure the 30 min removal efficiency of simulated radioactive aerosols as shown in Fig. 14(a). The results showed that the removal efficiency was further improved, and the 30 min removal rate reached 94.52%. Under the same conditions, the purification experiment results of CsCl simulated radioactive aerosol are shown in Fig. 14(b), and the purification effect of CsCl aerosol is close to that of ordinary aerosol. For CsCl aerosol with initial concentration greater than 10000 μg/cm^3, the purification efficiency of 30 min can still reach 94.07%, and the CRAES can purify radioactive aerosol at a relatively high level.

Removal mechanistic analysis

Research has shown that the root cause of the low collection efficiency of fine particulate matter is the uncontrollable fluid drag force. Therefore, increasing the particle size of fine particulate matter so that the uncontrollable fluid drag force is no longer the dominant force can greatly improve the collection efficiency of fine particulate matter[32]. In a supersaturated environment,

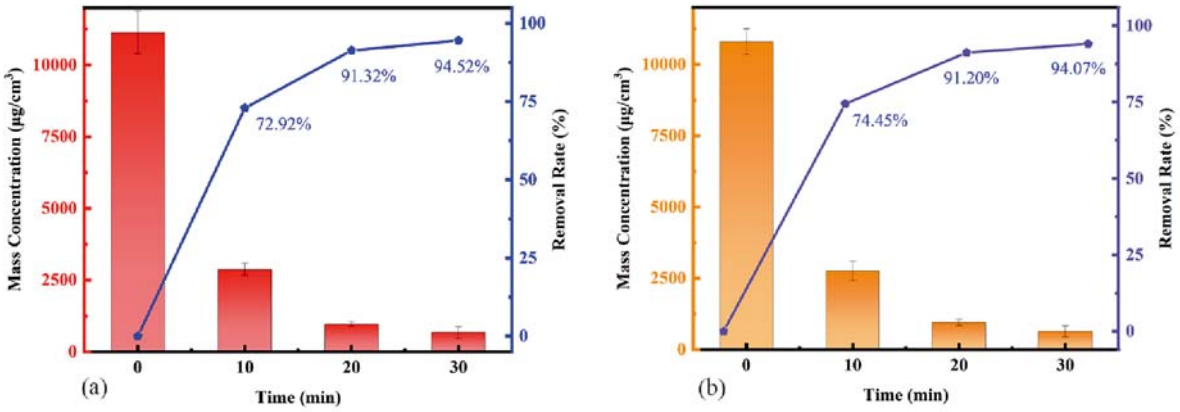


Figure 14. Optimum composite inhibitor removal results (a) incense simulated aerosol (b) CsCl simulated radioactive aerosol

the critical nucleation radius of water vapour containing particulate matter decreases, making it easier for fine particulate matter to reach the critical state. In the same situation, a larger number of fine particles reach a critical state[33]. With the addition of a composite inhibitor, the interaction includes static electricity and adsorption between the composite inhibitor and particulate matter can make it easier for the nucleus to break out of the unstable state, a phenomenon that is more pronounced with the addition of surfactants[34]. Under all additions, the purification of radioactive aerosol achieved a good effect. The CRAES removal mechanism can be outlined as follows: in the relative humidity-supersaturated environment achieved with the ultrasound atomization unit, the saturated water vapour heterogeneously condenses on the surface of fine particulate matter, which achieves a new phase state, produces an initial nucleus and activates the condensed nodules. New nucleus with radii greater than the critical nucleus radius will spontaneously increase in size due to water vapour condensation, achieving the growth of the concentrated nodules[37]. Fine particulate agglomerates increase in size and then pass through a specially designed cloud-type elimination unit, thus achieving efficient removal of radioactive aerosol particulate matter.

CONCLUSIONS

In this study, a self-designed and self-constructed experimental platform using water as an inhibitor achieved a 74.21% removal rate for simulated radioactive aerosols. A homemade composite was added to the ultrasound atomization unit, and five different concentrations were set at 1 mg/L, 2 mg/L, 5 mg/L, 10 mg/L and 20 mg/L. The best removal efficiency was achieved at a concentration of 2 mg/L, with a rate of 93.04%. At concentrations below 2 mg/L, the removal rate was 90.51%, and when the concentration was above 2 mg/L, the rate continued to decrease. The addition of PVA surfactant to the composite at the optimum concentration increased the removal rate at 10 min by 11.32%. The remaining four surfactants did not produce a significant enhancement effect. Among the five concentrations studied, 0.2 g/L PVA solution had the best enhancement effect on the removal efficiency at 10 min. This experiment concludes that the use of a composite inhibitor consisting of 2 mg/L FeOOH/rGO composite and 2 g/L PVA surfactant in a CRAES under the present method can achieve the maximum removal efficiency of simulated radioactive aerosols with a 30 min removal rate of 94.52%. The purification efficiency of CsCl simulated radioactive aerosol can reach 94.07%.

A new radioactive aerosol purification method was explored. CRAES coupled with the high-adsorption-capacity FeOOH/rGO composite inhibitor, which has no cartridges and less secondary contamination compared with existing technologies, it has broad application potential in collaborative treatment of radioactive aerosols. The method provides a way of thinking, researcher can further study the principle, select other efficient materials, perfect the method to form a new technology. However, the large footprint of the equipment is his limiting factor. The method can be applied in the confined space with potentially dangerous radioactivity, combined with the exhaust system at the end, to provide emergency treatment in the event of radioactive aerosol leakage, and is usually used for air purification, killing two birds with one stone.

ACKNOWLEDGMENT

This project is supported by National Natural Science Foundation of China (NSFC) (No.21875281).

LITERATURE CITED

1. Pang, C.X., You, H.H., Liang, L.L., Lin, X.Y., Zhang, Y.P., Zhang, H., Pan, X.H., Hu, Y., Chen, Y., Luo, X.G. & Wang, H.J. (2023). Bamboo pulp-based electret fiber aerogel with enhanced electret performance by P-phenylenediamine modification for simulated radioactive aerosol purification in confined spaces. *Colloids Surf. A Physicochem. Eng. Asp.*, 658, 130502. DOI: 10.1016/j.colsurfa.2022.130502.

2. Xue, Y., Chen, J., Liu, P., Gao, J.Z., Gui, Y.Y., Cheng, W.T., Mu, F.Q. & Yan, Y.D. (2022). An efficient and high-capacity porous functionalized-membranes for uranium recovery from wastewater. *Colloids Surf. A Physicochem. Eng. Asp.*, 647. DOI: 10.1016/J.COLSURFA.2022.129032.

3. Dong, X.A., Cw, A., Wei, D.A. & Hwa, B. (2020). Modelling dispersion of radioactive aerosols and occupational dose assessment of workers in a large nuclear plant industrial workshop with a stratified air conditioning system-sciencedirect. *Environ. Technol. Innov.*, 19. DOI: 10.1016/j.eti.2020.100828.

4. Lin, L., Chen, H., Lin, L. & Xu, Q. (2009). The literature review of radioactive aerosol purification. *Ind. Saf. Environ. Prot.*, 35, 1–3.

5. Lee, M.H., Yang, W., Chae, N. & Choi, S. (2019). Performance assessment of hepa filter against radioactive aerosols from metal cutting during nuclear decommissioning. *Nucl. Eng. Technol*., 52(5). DOI: 10.1016/j.net.2019.10.017.

6. El-Hussein, A. (2005). A study on natural radiation exposure in different realistic living rooms, *J. Environ. Radioact.*, 79, 355–367. DOI: 10.1016/j. jenvrad.2004.08.009.

7. Tripathi S.N. & Harrision R.G. (2001). Scavenging of electrifiedradioactive aerosol. *Atmos. Environ*., 35(33), 5817–5821. DOI: 10.1016/s1352-2310(01)00299-0.

8. Ren, H.Y., Li, J., Yu, F. & Liang, S.L. (2020). Current situation and prospect of radioactive aerosol removal technology. *Environ. Sci. Manag*., 45, 92–96. DOI: 10.3969/j. issn.1673–1212.2020.10.020.

9. Yang, T., Liu, Y. & Xing, P. (2003). Study on filtration efficiency of glass fiber filter for aerosols. *Radiat. Prot*., 23, 49–54. DOI: 10.3321/j.issn:1000-8187.2003.01.009.

10. Wang, T., Wang, S. & Gao, Y. (2021). Emergency control and elinination of radioactive aerosol diffusion in environmental pollution accidents. *Nucl. Saf.* 20, 17–24. DOI: 10.16432/j. cnki.1672-5360.2021.03.004.

11. Wang, L.J., Xu, X.C., Niu, X.H. & Pan, J.M. (2021). Colorimetric detection and membrane removal of arsenate by a multifunctional L-arginine modified FeOOH. *Sep. Purif. Technol*., 258, 118021. DOI: 10.1016/j.seppur.2020.118021.

12. Ding, S.J., Lu, J.W., Ding, Z.C., Li, N., Fu, F.L. & Tang, B. (2016). Cr (VI) removal by mesoporous FeOOH polymorphs: performance and mechanism. *RSC Adv.*, 6(84). DOI: 10.1039/c6ra14522a.

13. U.S. (2002). Department of Energy. Innovative technology summary report: fog and strip decontamination technology for use in D&D environments. LANL Release Number: LAUR-03-1558.

14. Berger, C., Song, Z.M., Li, T.B. & Ogbazghi, A.Y. (2004). Ultrathin Epitaxial Graphite: 2D Electron Gas roperties and a Route toward Graphene-based Nanoelectronics. *J. Phys. Chem*., 108(52), 19912–19916. DOI: 10.1021/jp040650f.

15. Nair, R.R., Blake, P. & Grigorenko, A.N. (2008). Fine Structure Constant Denes Visual Transparency of Graphene. *Sci*., 320, 1308. DOI: 10.1126/science.1156965.

16. Ren, J., Cao, T., Yang, X. & Tao, L. (2020). Ultrafiltration treatment of wastewater contained heavy metals complexed with palygorskite. *Pol. J. Chem. Technol*., 22(4), 1–9. DOI: 10.2478/pjct-2020-0031.

17. Abdel daiem, M., Sánchez-Polo, M., Rashed, A., Kamal, N. & Said, N. (2019). Adsorption mechanism and modelling of hydrocarbon contaminants onto rice straw activated carbons. *Pol. J. Chem. Technol.*, 21(4), 1–12. DOI: 10.2478/pjct-2019-0032.

18. Wang, B., Li, S.Q., Dong, S.J., Xin, R.B., Jin, R.Z., Zhang, Y.M., Dong, K.J. & Jiang, Y.C. (2018). A New Fine Particle Removal Technology: Cloud-Air-Purifying. *Ind. Eng. Chem. Res*., 57(34), 11815–11825. DOI: 10.1021/acs.iecr.8b03034.

19. Hummers, W.S. & Offeman, R.E., (1958). Preparation of graphitic oxide. *J. Am. Chem. Soc.*, 80, 1339.

20. Su, J., Jia, Y., Shi, M.L., Shen, K.K., & Zhang, J.Q. (2022). Highly efficient unsymmetrical dimethylhydrazine removal from wastewater using MIL-53(Al)-derived carbons: Adsorption performance and mechanisms exploration. *J. Environ. Chem. Eng.*, 10(6), 108975. DOI: 10.1016/j.jece.2022.108975.

21. Zou, Z.G., Yu, H.J., Long, F. & Fan, Y.H. (2011). Preparation of Graphene Oxide by Ultrasound-Assisted Hummers Method. *Chin. J. Inorg. Chem.,* 27(09):1753–1757.

22. Zhou, Q., Lin, Y.X., Shu, J., Zhang, K.Y., Yu, Z.Z. & Tang, D.P. (2017). Reduced graphene oxide-functionalized FeOOH for signal-on photoelectrochemical sensing of prostate-specific antigen with bioresponsive controlled release system. *Biosens. and Bioelectron*., 98, 15–21. DOI: 10.1016/j. bios.2017.06.033.

23. Kirpalani, D.M. & Suzuki, K. (2011). Ethanol enrichment from ethanol-water mixtures using high frequency ultrasonic atomization. *Ultrason. Sonochem*., 18(5), 1012–1017. DOI: 10.1016/j.ultsonch.2010.05.013.

24. Trinh, V., Van, H., Pham, Q., Trinh, M. & Bui, H. (2020). Treatment of medical solid waste using an Air Flow controlled incinerator. *Pol. J. Chem. Technol.*, 22(1) 29–34. DOI: 10.2478/pjct-2020-0005.

25. Zhou, Y., Bao, Q.L., Tang, L.A.L., Zhong, Y.L. & Loh, K.P. (2009). Hydrothermal Dehydration for the "Green" Reduction of Exfoliated Graphene Oxide to Graphene and Demonstration of Tunable Optical Limiting Properties. *Chem. of Mater*., 21(13), 2950–2956. DOI: 10.1021/cm9006603.

26. Qiu, J.X., Zhang, P., Ling, M., Li, S., Liu, P.R., Zhao, H.J. & Zhang, S.Q. (2012). Photocatalytic Synthesis of TiO2 and Reduced Graphene Oxide Nanocomposite for Lithium Ion Battery. *ACS Appl. Mater. Interface.*, DOI: 10.1021/am300722d.

27. Han, Y., & Lu, Y. (2009). Characterization and electrical properties of conductive polymer/colloidal graphite oxide nanocomposites. *Compos. Sci. Technol.*, 69(7–8), 1231–1237. DOI: 10.1016/j.compscitech.2009.02.028.

28. Yang, Z., Liu, X., Liu, X., Wu, J. & Yu, Z. (2021). Preparation of β-cyclodextrin/graphene oxide and its adsorption properties for methylene blue. *Colloids Surf., B*, 111605. DOI: 10.1016/j.colsurfb.2021.111605.

29. Lei, C., Wen, F., Chen, J., Chen, W. & Wang, B. (2021). Mussel-inspired synthesis of magnetic carboxymethyl chitosan aerogel for removal cationic and anionic dyes from aqueous solution. *Polym.*, 213(26), 123316. DOI: 10.1016/j. polymer.2020.123316.

30. Travlou, N.A., Kyzas, G.Z., Lazaridis, N.K., & Deliyanni, E.A. (2013). Functionalization of Graphite Oxide with Magnetic Chitosan for the Preparation of a Nanocomposite Dye Adsorbent. *Langmuir*, 29(5), 1657–1668. DOI: 10.1021/la304696y.

31. Geng, F.X., Zhao, Z.G., Geng, J.X., Cong, H.T. & Cheng H.M. (2007). A simple and low-temperature hydrothermal route for the synthesis of tubular α-FeOOH. *Mater. Lett.*, 61(26), 4794–4796. DOI: 10.1016/j.matlet.2007.03.036.

32. Zhang, J.Q., Jia, Y. & Lv, X.M. 2023. View of the use of Cloud-Air-Purifying in radioactive aerosol purification. *Appl. Chem. Ind.* 01, 223–226+232. DOI: 10.16581/j.cnki.issn1671-3206.20221214.003.

33. Pramod, K., Paul, A.B. & Klaus, W. 2020. Aerosol Measurement: Principles, Techniques and Applications. Beijing: Chemical Industry Press.

34. Striolo, A. (2019). Studying surfactants adsorption on heterogeneous substrates. *Curr. Opin. Chem. Eng*. 23, 115–122. DOI: 10.1016/j.coche.2019.03.009.

35. Xu, J. C., Zhang, J. & Yu, Y. (2016). Characteristics of vapor condensation on coal-fired fine particles. *Energy & Fuels.* 30(3), 1822–1828. DOI: 10.1021/acs. energyfuels. 5b02200.

36. Bao, J.J., Yang, L.J. & Guo, W.W. (2012). Improving the removal of fine particles in the WFGD system by adding wetting agent. *Energy & Fuels*. 26(8), 4924–4931. DOI: 10.1021/ef3007195.

37. Mason, B.J. (1978). Cloud physics. Beijing: Science Press.